



OPEN

# Charge-transfer-based Gas Sensing Using Atomic-layer MoS<sub>2</sub>

SUBJECT AREAS:

TWO-DIMENSIONAL  
MATERIALS  
MATERIALS CHEMISTRY

Byungjin Cho<sup>1\*</sup>, Myung Gwan Hahm<sup>1\*</sup>, Minseok Choi<sup>2</sup>, Jongwon Yoon<sup>3</sup>, Ah Ra Kim<sup>1</sup>, Young-Joo Lee<sup>1</sup>, Sung-Gyu Park<sup>1</sup>, Jung-Dae Kwon<sup>1</sup>, Chang Su Kim<sup>1</sup>, Myungkwon Song<sup>1</sup>, Yongsoo Jeong<sup>4</sup>, Kee-Seok Nam<sup>1</sup>, Sangchul Lee<sup>5</sup>, Tae Jin Yoo<sup>3</sup>, Chang Goo Kang<sup>6</sup>, Byoung Hun Lee<sup>3</sup>, Heung Cho Ko<sup>3</sup>, Pulickel M. Ajayan<sup>7</sup> & Dong-Ho Kim<sup>1</sup>

Received

1 October 2014

Accepted

31 December 2014

Published

27 January 2015

Correspondence and requests for materials should be addressed to B.C. (bjcho@kims.re.kr); M.G.H. (mghahm@kims.re.kr) or D.-H.K. (dhkim2@kims.re.kr)

\* These authors contributed equally to this work.

<sup>1</sup>Advanced Functional Thin Films Department, Surface Technology Division, Korea Institute of Materials Science (KIMS), 797 Changwondaero, Sungsan-Gu, Changwon, Gyeongnam 642-831, Republic of Korea, <sup>2</sup>Advanced Characterization and Analysis Group, Korea Institute of Materials Science (KIMS), 797 Changwondaero, Sungsan-Gu, Changwon, Gyeongnam 642-831, Republic of Korea, <sup>3</sup>School of Materials Science and Engineering, Gwangju Institute of Science and Technology (GIST), 261 Cheomdan-gwagiro, Buk-Gu, Gwangju 500-712, Republic of Korea, <sup>4</sup>Electrochemistry Department, Korea Institute of Materials Science (KIMS), 797 Changwondaero, Sungsan-Gu, Changwon, Gyeongnam 642-831, Republic of Korea, <sup>5</sup>Department of Chemical Engineering and Materials Science, Stevens Institute of Technology, Hoboken, New Jersey 07030, United States, <sup>6</sup>Cambridge Graphene Center, University of Cambridge, 9 JJ Thomson Avenue, Cambridge, United Kingdom, <sup>7</sup>Department of Materials Science and NanoEngineering, Rice University, 6100 Main Street, Houston, Texas 77005, USA.

**Two-dimensional (2D) molybdenum disulphide (MoS<sub>2</sub>) atomic layers have a strong potential to be used as 2D electronic sensor components. However, intrinsic synthesis challenges have made this task difficult. In addition, the detection mechanisms for gas molecules are not fully understood. Here, we report a high-performance gas sensor constructed using atomic-layered MoS<sub>2</sub> synthesised by chemical vapour deposition (CVD). A highly sensitive and selective gas sensor based on the CVD-synthesised MoS<sub>2</sub> was developed. *In situ* photoluminescence characterisation revealed the charge transfer mechanism between the gas molecules and MoS<sub>2</sub>, which was validated by theoretical calculations. First-principles density functional theory calculations indicated that NO<sub>2</sub> and NH<sub>3</sub> molecules have negative adsorption energies (i.e., the adsorption processes are exothermic). Thus, NO<sub>2</sub> and NH<sub>3</sub> molecules are likely to adsorb onto the surface of the MoS<sub>2</sub>. The *in situ* PL characterisation of the changes in the peaks corresponding to charged trions and neutral excitons via gas adsorption processes was used to elucidate the mechanisms of charge transfer between the MoS<sub>2</sub> and the gas molecules.**

Over the past few decades, metal oxide semiconductors have been applied as conventional chemical sensing materials because of their high sensitivity and relatively low cost<sup>1–3</sup>. However, they still have some critical drawbacks. First, metal oxide semiconductors exhibit poor sensitivity and selectivity at room temperature. This obstacle has led to the development of alternative materials such as carbon nanotubes<sup>4</sup>, graphene<sup>5</sup>, and transition metal dichalcogenides (TMDs)<sup>6–11</sup>. Recently, 2D TMDs have attracted much attention for use in next-generation nanoelectronic devices<sup>12–14</sup>, with a single-layer MoS<sub>2</sub> transistor having been reported to exhibit outstanding performance<sup>15</sup>. The intrinsic merits of TMDs, including their high surface-to-volume ratio and semiconducting properties, have accelerated the development of a diverse range of applications of these materials as chemical sensors. A recent flurry of research involving MoS<sub>2</sub>-based gas detection has mitigated the wide chasm between metal oxide materials and alternatives<sup>6–11</sup>. However, the fundamental mechanism of chemical sensing using MoS<sub>2</sub> remains unclear, limiting its practical applications. Here, we demonstrate highly sensitive and selective gas detection of NO<sub>2</sub> and NH<sub>3</sub> using uniform wafer-scale MoS<sub>2</sub> nanofilms synthesised by thermal chemical vapour deposition (CVD). We elucidate the charge transfer mechanism of MoS<sub>2</sub> gas adsorption using *in situ* photoluminescence (PL) and computational calculations involving first-principles density functional theory. The peak intensities from the positively charged trions (A<sup>+</sup>) and neutral excitons (A<sup>0</sup>) in the PL spectrum show trade-off phenomena by adsorption of each different gas molecule (NO<sub>2</sub> or NH<sub>3</sub>) onto the MoS<sub>2</sub>. The electron depletion of MoS<sub>2</sub> by NO<sub>2</sub> adsorption leads to an increase in the intensity of the A<sup>+</sup> peak and a suppression of the intensity of the A<sup>0</sup> peak, whereas electron accumulation by NH<sub>3</sub> adsorption suppresses the intensity of the A<sup>+</sup> peak and increases the intensity of the A<sup>0</sup> peak. These *in situ* PL characterisation results clarify the mechanisms of



charge transfer between the MoS<sub>2</sub> and the gas molecules. These findings will help to implement future gas sensing technologies using diverse two dimensional TMDs nanomaterials.

## Results

**Wafer-scale synthesis of atomic-layered MoS<sub>2</sub>.** Most approaches use direct/indirect sulphurisation of Mo-containing thin films to synthesise atomic-layered MoS<sub>2</sub> thin films. The precursor is a key factor in the synthesis of MoS<sub>2</sub>. In previous studies, most authors adopted one of three precursors: molybdenum thin films<sup>16</sup>; molybdenum trioxide<sup>17</sup>; or ammonium thiomolybdate<sup>18</sup>. However, previous methods have involved complex precursor preparations, yielding films with inconsistent quality. In our search for strategies for synthesising uniform wafer-scale MoS<sub>2</sub> (see schematic in Fig. 1a), we have focused on the development of a thermal CVD system and process. Atomic-layered MoS<sub>2</sub> was grown using molybdenum trioxide (MoO<sub>3</sub>) deposited onto a sapphire substrate and a sulphur powder source. The sublimated sulphur served as a precursor to sulphurise the MoO<sub>3</sub> film. To achieve our overall goal of preparing MoS<sub>2</sub> films of consistent quality on the desired substrates, we turned our attention to pressure control during the CVD reaction. A recent report indicated that an increase in the amount of either Mo or S atoms results in increased formation of energetically favourable defects on the MoS<sub>2</sub> surface during film growth<sup>19</sup>. Thus, we systematically controlled the reaction pressure to provide sufficient sublimated sulphur using a custom-made automatic pressure control system (Supplementary Fig. S1).

The new CVD system design was very effective for the uniform synthesis of MoS<sub>2</sub> films on 2-inch sapphire substrates, as illustrated in Fig. 1b. Cross-sectional transmission electron microscopy (TEM) was used to examine the number of layers formed by CVD (Fig. 1c).

The MoS<sub>2</sub> films contained double, triple, and, in some cases, more than three layers (additional TEM images, TEM energy-dispersive X-ray spectroscopy (EDS) maps, TEM EDS point spectra, atomic force microscopy images, X-ray photoelectron spectra, and absorption spectra are provided in Supplementary Figs. S2–7). The Raman spectrum in Fig. 1d shows the in-plane vibrational mode of the Mo and S atoms (E<sub>2g</sub>) and the out-of-plane vibrational mode of S atoms (A<sub>1g</sub>) in the as-synthesised MoS<sub>2</sub> films<sup>20</sup>. The difference in peak position ( $\Delta$ ) between the E<sub>2g</sub> and A<sub>1g</sub> bands, which is a strong indicator of the number of layers, was approximately 22.9. This result indicates that the as-synthesised MoS<sub>2</sub> was mainly composed of three layers<sup>18,21,22</sup>. To confirm the wafer-scale synthesis of MoS<sub>2</sub>, we conducted a large-scale structural analysis using Raman mapping and an imaging technique. The Raman mapping area was 50 × 50 μm<sup>2</sup> with 0.3 μm steps (the original Raman mapping spectra are shown in Supplementary Fig. S8). The corresponding Raman images revealed the spatial distribution of MoS<sub>2</sub> over a 250-μm<sup>2</sup> area of the substrate (Figs. 1e and f). The blue and red models show the spatial distributions of the E<sub>2g</sub> and A<sub>1g</sub> bands, respectively. The as-synthesised MoS<sub>2</sub> was highly uniform over a large area of the surface (Figs. 1e and f). Thus, systematic pressure control during the CVD process resulted in highly uniform MoS<sub>2</sub> films on the wafer scale.

**Gas detection characteristics of the MoS<sub>2</sub> gas sensor.** The uniform atomic-layered MoS<sub>2</sub> films were used for gas molecule detection (Fig. 2a). Transient resistance responses were investigated using two analyte gases (NO<sub>2</sub> or NH<sub>3</sub> at concentrations from 1.2 to 50 ppm). The gas sensitivity was calculated using  $\Delta R/R_a = (R_g - R_a)/R_a$ , where R<sub>a</sub> and R<sub>g</sub> represent the resistances of the device to air and the analyte gas, respectively. In the NO<sub>2</sub> gas mode, the resistance increased (positive sensitivity) (Fig. 2b). The NO<sub>2</sub>

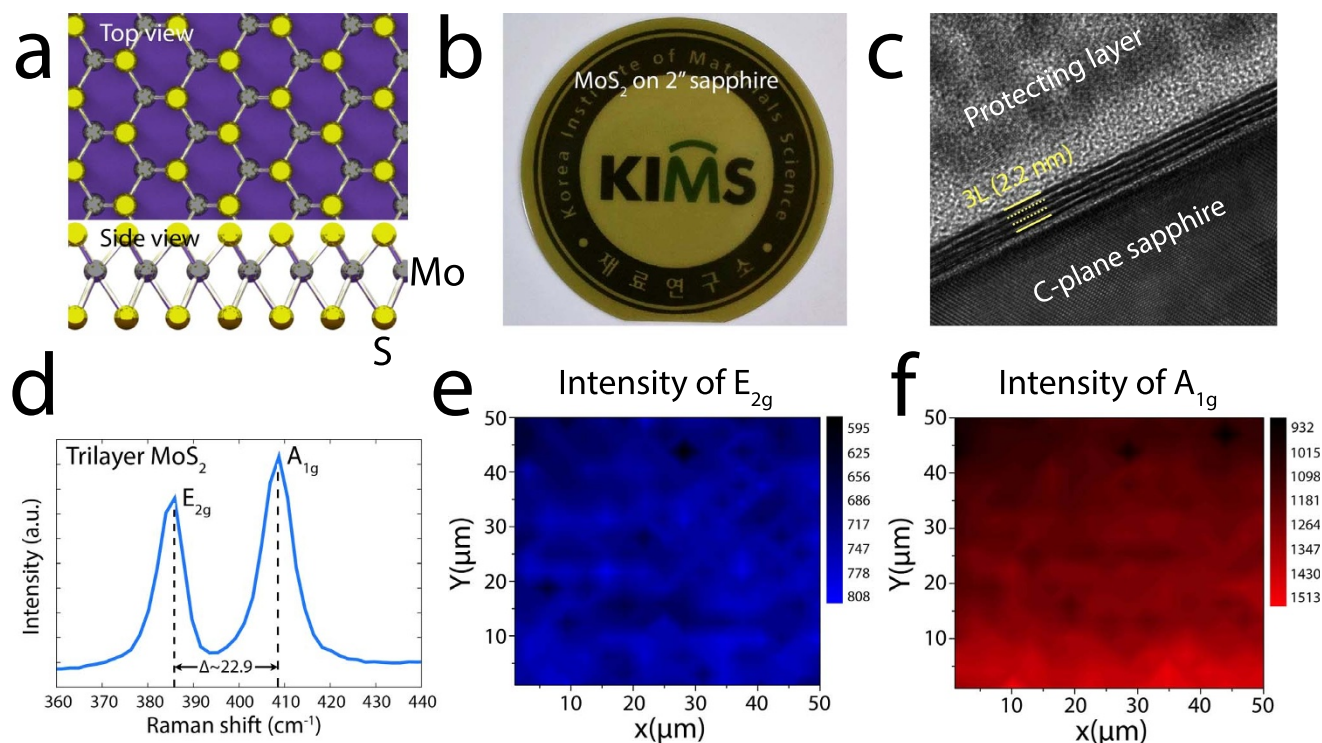


**Figure 1 | Large-scale synthesis of MoS<sub>2</sub>.** (a) Schematic of the atomic-layered MoS<sub>2</sub>. The quasi-2D MoS<sub>2</sub> was occupied by one Mo (a trigonal prismatic structure) and two S atoms (hexagonal planes). (b) Image of the as-synthesised MoS<sub>2</sub> film on the 2-inch sapphire substrate. The as-synthesised MoS<sub>2</sub> film was semi-transparent. (c) Cross-sectional TEM images of the as-grown MoS<sub>2</sub> films. The image clearly demonstrates that the synthesised MoS<sub>2</sub> films consisted of three layers of MoS<sub>2</sub>. (d) Raman spectrum of the triple-layered MoS<sub>2</sub>. The spectrum reveals a strong in-plane vibrational mode for the Mo and S atoms (E<sub>2g</sub>) and an out-of-plane vibrational mode for the S atoms (A<sub>1g</sub>). The peak position difference ( $\Delta$ ) between the E<sub>2g</sub> and A<sub>1g</sub> bands is approximately 22.9, indicating triple-layered MoS<sub>2</sub>. (e, f) Raman maps of E<sub>2g</sub> (blue) and A<sub>1g</sub> (red), respectively. The Raman mapping area was 50 × 50 μm<sup>2</sup> with 0.3 μm steps. The Raman images show the spatial distribution on the surface of the substrates.

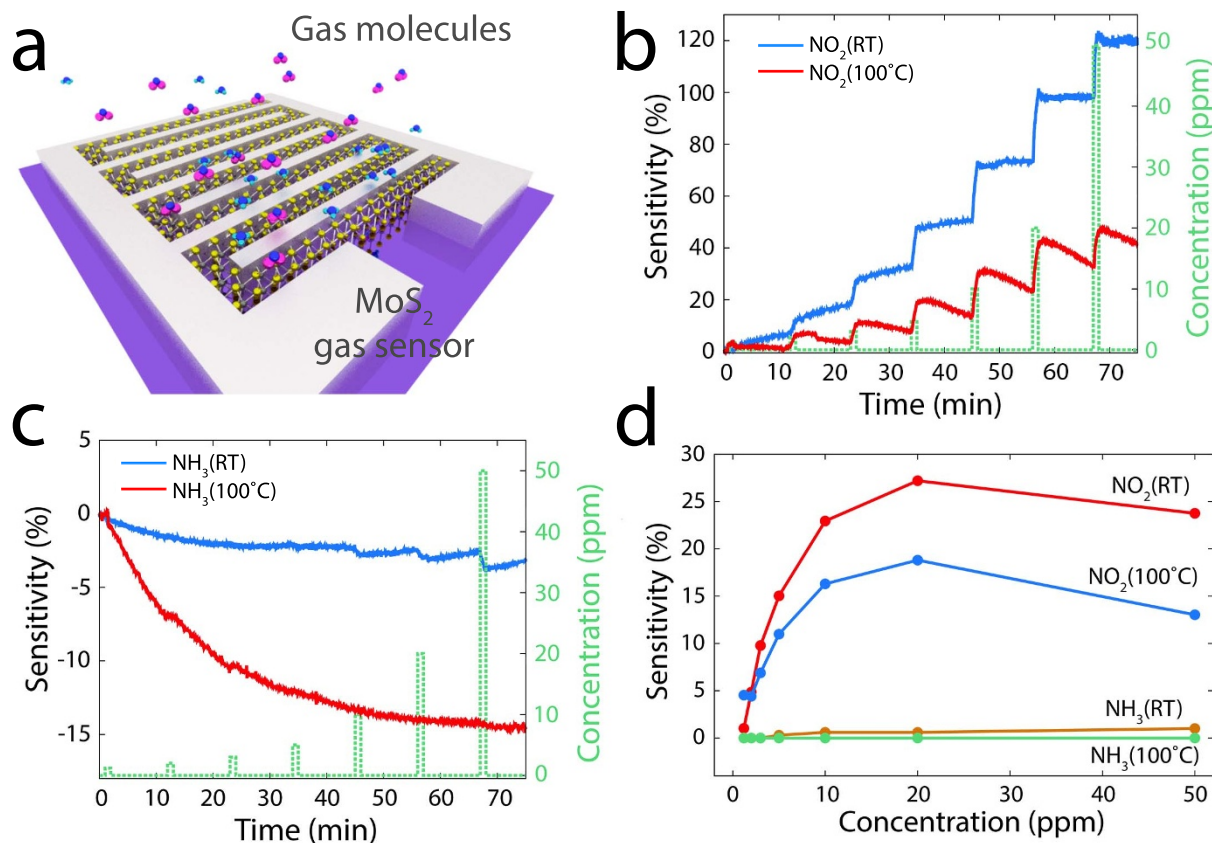


**Figure 2** | Gas-sensing using the MoS<sub>2</sub> device. (a) 3D schematic of the MoS<sub>2</sub> gas-sensing device for NO<sub>2</sub> and NH<sub>3</sub>. (b) Transient NO<sub>2</sub> gas response at 1.5 to 50 ppm gas at operating temperatures of RT and 100°C. In the NO<sub>2</sub> gas mode, the resistance increases (positive sensitivity). The recovery rate of NO<sub>2</sub> is higher at 100°C than at RT. (c) The transient NH<sub>3</sub> gas response at 1.5 to 50 ppm gas at operating temperatures of RT and 100°C. The resistance decreases with the adsorption of NH<sub>3</sub> gas molecules (negative sensitivity). The NH<sub>3</sub> sensing signal is negligible at 100°C. (d) Comparison of the NO<sub>2</sub> and NH<sub>3</sub> sensitivities at different gas concentrations and operating temperatures. The highest selectivity of NO<sub>2</sub> to NH<sub>3</sub> was obtained when the concentration reached 20 ppm at 100°C.

sensitivity values were comparable to those in a previous report<sup>8</sup>. NO<sub>2</sub> acts as an electron acceptor, resulting in p-doping (Supplementary Fig. S12). The NO<sub>2</sub> molecules on the surface of MoS<sub>2</sub> bring the Fermi level closer to the valence-band edge. During the desorption process, thermal energy (heating to 100°C) enhances the rate of desorption of the NO<sub>2</sub> molecules from the MoS<sub>2</sub> film (Fig. 2b, red line). We next compared the gas sensing characteristics for NH<sub>3</sub> to those for NO<sub>2</sub> (Fig. 2c). In contrast to the resistance recorded for NO<sub>2</sub> molecules, the resistance of the MoS<sub>2</sub> sensing device decreased with the adsorption of NH<sub>3</sub> gas molecules, i.e., negative sensitivity was observed. NH<sub>3</sub> acts as an electron donor (i.e., n-doping) such that it shifts the Fermi level of the MoS<sub>2</sub> to the conduction-band edge. However, theoretical calculations indicated that the Fermi-level shift induced by the NH<sub>3</sub> molecules is negligible (Supplementary Fig. S12). The measured overall NH<sub>3</sub> sensitivities were lower than those of NO<sub>2</sub> (Figs. 2b and c) because of the smaller charge transfer of NH<sub>3</sub> compared to that of NO<sub>2</sub><sup>23</sup>. The dependence of the gas response on the gas concentration at different operating temperatures is plotted in Fig. 2d. The surface chemical reaction between the MoS<sub>2</sub> channel and the NO<sub>2</sub> molecules saturated at approximately 20 ppm, irrespective of the operating temperature (Fig. 2d, red and blue lines). By contrast, in the case of NH<sub>3</sub>, the sensitivity at RT gradually increased from 5 to 50 ppm and the sensitivity under 5 ppm was undetectable. However, the sensing signal at 100°C was imperceptible at all concentrations (Supplementary Fig. S9). Thus, the recovery rate of NO<sub>2</sub> at 100°C is clearly superior to that of NH<sub>3</sub>, which is closely related to the faster desorption process of NO<sub>2</sub> molecules as a result of the thermal

energy<sup>24,25</sup>. At 20 ppm and 100°C, we obtained the best selectivity for NO<sub>2</sub> relative to NH<sub>3</sub> (~400% increase compared to that at RT).

**In situ photoluminescence of the MoS<sub>2</sub>-based gas sensor.** To explore the gas adsorption characteristics of the MoS<sub>2</sub>, we adopted theoretical and experimental approaches. First-principles density functional theory (DFT) calculations were conducted using the screened hybrid functional of Heyd-Scuseria-Ernzerhof with the D2 correction for van der Waals interactions<sup>26,27</sup> (see the detailed methods in the Supplementary Information). To simulate NO<sub>2</sub> and NH<sub>3</sub> adsorption onto the MoS<sub>2</sub> monolayer, supercells containing 16 Mo and 32 S atoms with NO<sub>2</sub> and NH<sub>3</sub> were employed using a 2 × 2 × 1 k-point grid. The most stable configurations of NO<sub>2</sub> and NH<sub>3</sub> reported in a recent study that compared the total energy between different adsorption configurations<sup>28</sup> were considered. The NO<sub>2</sub> and NH<sub>3</sub> molecules were preferentially adsorbed onto the top of the hexagon of the MoS<sub>2</sub><sup>28</sup> (Figs. 3a and b). The adsorption energies of the NO<sub>2</sub> and NH<sub>3</sub> gas molecules were evaluated using  $E_a = E_{(MoS_2 - molecule)} - [E_{(MoS_2)} + E_{(molecule)}]$ , where  $E_{(MoS_2 - molecule)}$  is the total energy of a supercell containing both an MoS<sub>2</sub> monolayer and a gas molecule (NO<sub>2</sub> or NH<sub>3</sub>),  $E_{(MoS_2)}$  is the total energy of the host MoS<sub>2</sub> supercell, and  $E_{(molecule)}$  is the total energy of a supercell containing a gas molecule. The calculated adsorption energies of NO<sub>2</sub> and NH<sub>3</sub> were -0.14 eV and -0.16 eV, respectively. These values were ~0.1 eV smaller than the values obtained using the local density approximation (LDA) because the LDA functional overestimates the adsorption energy<sup>28</sup>. The negative adsorption energies indicate that the adsorption process is exothermic. Thus,

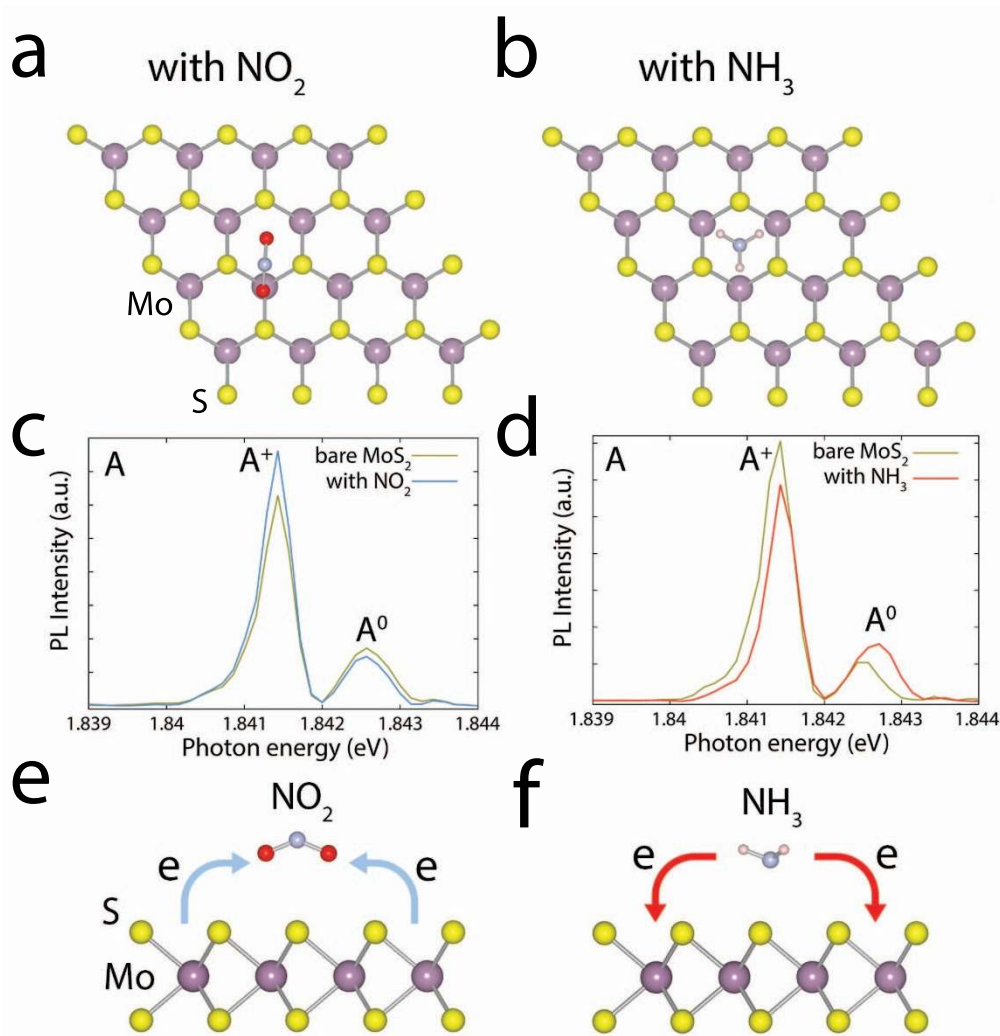


**Figure 3 | Adsorption configurations and *in situ* PL.** (a, b) Top views of the most favourable configurations for NO<sub>2</sub> (a) and NH<sub>3</sub> (b) on the MoS<sub>2</sub>. The calculated adsorption energies were  $-0.14$  eV for NO<sub>2</sub> and  $-0.16$  eV for NH<sub>3</sub>. The negative adsorption energies indicate that the adsorption process is exothermic, indicating that NO<sub>2</sub> and NH<sub>3</sub> molecules are likely to be adsorbed onto the surface of the MoS<sub>2</sub>. (c, d) *In situ* PL spectra recorded from the MoS<sub>2</sub> with NO<sub>2</sub> (c) and NH<sub>3</sub> (d) molecules. The overall intensity of the PL spectra changes in the presence of NO<sub>2</sub> and NH<sub>3</sub> molecules. The PL intensities of the A<sup>+</sup> trions and A<sup>0</sup> excitons are either suppressed or increased by changes in the concentrations of the charge carriers. (e, f) Schematics of the charge density differences for MoS<sub>2</sub> in the presence of NO<sub>2</sub> (e) and NH<sub>3</sub> (f) gas molecules. NO<sub>2</sub> molecules on the surface of MoS<sub>2</sub> act as electron acceptors, whereas NH<sub>3</sub> molecules act as electron donors.

NO<sub>2</sub> and NH<sub>3</sub> molecules are likely to be adsorbed onto the surface of MoS<sub>2</sub>.

Next, we turned our attention to the *in situ* characterisation of PL to study the sensing mechanism in depth. The high temperature during film growth can induce unintentional defects on the substrate/MoS<sub>2</sub> interface. To prevent defects, we transferred the as-grown MoS<sub>2</sub> from the sapphire substrate to a SiO<sub>2</sub>/p + Si substrate. Interestingly, the atomic-layered MoS<sub>2</sub> transferred onto the SiO<sub>2</sub>/p + Si substrate exhibited opposite gas sensitivity (i.e., p-type behaviour) compared to the n-type behaviour of MoS<sub>2</sub> on the sapphire substrate (see Supplementary Fig. S13 for details). Dangling bonds at the semiconductor/substrate interface can redefine the effective Fermi levels within gap states, modulating the conductive properties of the MoS<sub>2</sub><sup>29</sup>. The dangling oxygen bonds on the SiO<sub>2</sub> surface can result in a p-type MoS<sub>2</sub> semiconductor<sup>29</sup>. In the *in situ* PL characterisation with the two analyte gases (see Supplementary Fig. S10 for details), we observed various intensity changes in the PL spectra for NO<sub>2</sub> and NH<sub>3</sub> molecules (Figs. 3c and d). The atomic-layered MoS<sub>2</sub> had two main PL peaks associated with the A and B excitons<sup>30</sup> (Supplementary Figs. S11). Spin-orbit coupling-induced valence-band

splitting can give rise to A and B excitons<sup>31</sup>. After the gas molecules are adsorbed, the PL intensities of the A and B excitons can either be suppressed or increased by changing the concentrations of the charge carriers<sup>32,33</sup>. We here focused on the signal peak of the A exciton. The relatively low-energy A exciton signal expands to two features: a trion of A<sup>-/+</sup> (two electrons to a hole, resulting in a negatively charged exciton, or an electron to two holes, resulting in a positively charged exciton) and a neutral exciton of A<sup>0</sup><sup>32,33</sup>. With the emergence of the trion, we assumed that the exciton is coupled to either another electron or to a hole at the Fermi level. In the case of MoS<sub>2</sub>, the A<sup>+</sup> and A<sup>0</sup> peaks correspond to the trions (1.8413 eV) and to the neutral excitons (1.8424 eV), respectively. The bare MoS<sub>2</sub> notwithstanding, the positive trion (in this case, an electron to two holes, resulting in positively charged excitons, A<sup>+</sup>) emission dominates the PL spectra because the bare MoS<sub>2</sub> on the SiO<sub>2</sub> substrate exhibits p-type characteristics, as previously mentioned<sup>32</sup>. As schematically shown in Fig. 3e, the NO<sub>2</sub> molecules on the surface of the MoS<sub>2</sub> act as electron acceptors (p-type dopants), whereas the NH<sub>3</sub> molecules act as electron donors (n-type dopants)<sup>28</sup>. By adsorp-



tion of NO<sub>2</sub> gas molecules, a neutral exciton (A<sup>0</sup>) can be converted into a quasi-particle (A<sup>+</sup>) because of excessive holes generated by electron extraction from the MoS<sub>2</sub><sup>34</sup>. As a result, the A<sup>+</sup> peak in the PL spectrum increases in intensity and the A<sup>0</sup> peak is suppressed (Fig. 3c). By contrast, when additional electrons are introduced from the NH<sub>3</sub> molecules, the intensity of the A<sup>+</sup> peak in the PL spectrum is suppressed because of dissociation of the positive trions from the neutral excitons, resulting in increasing neutral excitons (A<sup>0</sup>)<sup>35</sup>, as shown in Fig. 3d. The *in situ* PL characterisation clarifies the mechanisms of charge transfer between the MoS<sub>2</sub> and the gas molecules.

## Discussion

The gas sensing characteristics of wafer-scale layered MoS<sub>2</sub> fabricated by CVD were determined. The gas sensor based on the CVD-fabricated MoS<sub>2</sub> exhibited excellent sensitivity and high selectivity. The *in situ* PL characterisation and theoretical studies elucidated the charge-transfer mechanism between the gas molecules and the MoS<sub>2</sub>. In-depth PL studies verified that the electron depletion of the MoS<sub>2</sub> by NO<sub>2</sub> adsorption increased the intensity of the A<sup>+</sup> peak and suppressed that of the A<sup>0</sup> peak, whereas electron accumulation by NH<sub>3</sub> adsorption suppressed the intensity of the A<sup>+</sup> peak and increased that of the A<sup>0</sup> peak. Intensive PL characterisation clarified the charge transfer phenomena between the MoS<sub>2</sub> and the gas molecules. The results of this study will enable more extensive applications of gas sensing using two dimensional transition metal dichalcogenides nanomaterials.

## Methods

**CVD synthesis of the MoS<sub>2</sub> nanofilms.** MoS<sub>2</sub> nanofilms were synthesised using chemical vapour deposition (CVD) (Teraleader Co., Ltd., South Korea) (Supplementary Fig. S1). First, C-plane sapphire substrates were prepared using a typical cleaning process (sonication in acetone, isopropyl alcohol, and deionised water for 10 min each). MoO<sub>3</sub> films (5 nm) were deposited onto the clean substrates using a thermal evaporator. The pre-deposited MoO<sub>3</sub> samples were placed at the centre of the furnace, and ~1 g of sulphur powder, which was used as a sulphur precursor, was subsequently loaded into a quartz boat in an independently temperature-controllable flange heater located near the inlet of the furnace. The furnace and the flange heater were heated to ~850°C and ~180°C, respectively, for 1 h. The process was maintained for an additional 1 h under flowing Ar/H<sub>2</sub> gas (volume ratio: Ar:H<sub>2</sub> = 85:15%) at a chamber pressure of 760 torr. The MoO<sub>3</sub> film was converted into a MoS<sub>2</sub> nanofilm via a two-step reaction (the reduction of MoO<sub>3</sub> by hydrogen gas, followed by sulphurisation of the reduced MoO<sub>3</sub> with sublimated sulphur gases). Finally, the furnace was rapidly cooled to room temperature by opening the chamber box after the furnace was turned off.

**Fabrication of the MoS<sub>2</sub> sensing device.** The SiO<sub>2</sub> (300 nm)/C-plane sapphire was cleaned using a typical cleaning process (sequential sonication in acetone, isopropyl alcohol, and deionised water for 10 min each). A MoO<sub>3</sub> film (~5 nm thick) was patterned with an active shadow mask using a thermal evaporator. The patterned MoO<sub>3</sub> film was converted into a MoS<sub>2</sub> nanofilm by CVD. Using a thermal evaporator and a shadow mask with an interdigitated electrode array structure consisting of two opposing comb-shaped electrodes with a width of 400 μm and a gap of 100 μm, we deposited an Ag film (100 nm; used for the electrodes) onto the MoS<sub>2</sub> nanofilm. Detailed fabrication schemes are provided in Supplementary Fig. S14.

**Characterisation of CVD-synthesised MoS<sub>2</sub>, gas sensing, DFT calculations, *in situ* PL tests.** See the detailed methods in the Supplementary Information.

1. Fine, G. F., Cavanagh, L. M., Afonja, A. & Binions, R. Metal oxide semi-conductor gas sensors in environmental monitoring. *Sensors (Basel)*. **10**, 5469–5502 (2010).
2. Pearton, S. J. *et al.* Recent advances in wide bandgap semiconductor biological and gas sensors. *Prog. Mater. Sci.* **55**, 1–59 (2010).
3. Huang, J. & Wan, Q. Gas sensors based on semiconducting metal oxide one-dimensional nanostructures. *Sensors (Basel)*. **9**, 9903–9924 (2009).
4. Kong, J. Nanotube Molecular Wires as Chemical Sensors. *Science* **287**, 622–625 (2000).
5. Schedin, F. *et al.* Detection of individual gas molecules adsorbed on graphene. *Nat. Mater.* **6**, 652–655 (2007).
6. Late, D. J. *et al.* Sensing Behavior of Atomically Thin-Layered MoS<sub>2</sub> Transistors. *ACS Nano* **7**, 4879–4891 (2013).
7. Li, H. *et al.* Fabrication of single- and multilayer MoS<sub>2</sub> film-based field-effect transistors for sensing NO at room temperature. *Small* **8**, 63–67 (2012).

8. He, Q. *et al.* Fabrication of flexible MoS<sub>2</sub> thin-film transistor arrays for practical gas-sensing applications. *Small* **8**, 2994–2999 (2012).
9. Lee, K., Gatensby, R., McEvoy, N., Hallam, T. & Duesberg, G. S. High Performance Sensors Based on Molybdenum Disulfide Thin Films. *Adv. Mater.* **25**, 6699–6702 (2013).
10. Yao, Y. *et al.* High-concentration aqueous dispersions of MoS<sub>2</sub>. *Adv. Funct. Mater.* **23**, 3577–3583 (2013).
11. Perkins, F. K. *et al.* Chemical vapor sensing with monolayer MoS<sub>2</sub>. *Nano Lett.* **13**, 668–673 (2013).
12. Wang, Q. H., Kalantar-Zadeh, K., Kis, A., Coleman, J. N. & Strano, M. S. Electronics and optoelectronics of two-dimensional transition metal dichalcogenides. *Nat. Nanotechnol.* **7**, 699–712 (2012).
13. Ganatra, R. & Zhang, Q. Few-Layer MoS<sub>2</sub>: A Promising Layered Semiconductor. *ACS Nano* **8**, 4074–4099 (2014).
14. Jariwala, D., Sangwan, V. K., Lauhon, L. J., Marks, T. J. & Hersam, M. C. Emerging Device Applications for Semiconducting Two-Dimensional Transition Metal Dichalcogenides. *ACS Nano* **8**, 1102–1120 (2014).
15. Radisavljevic, B., Radenovic, A., Brivio, J., Giacometti, V. & Kis, A. Single-layer MoS<sub>2</sub> transistors. *Nat. Nanotechnol.* **6**, 147–150 (2011).
16. Lee, Y. *et al.* Synthesis of wafer-scale uniform molybdenum disulfide films with control over the layer number using a gas phase sulfur precursor. *Nanoscale* **6**, 2821–2826 (2014).
17. Lin, Y.-C. *et al.* Wafer-scale MoS<sub>2</sub> thin layers prepared by MoO<sub>3</sub> sulfurization. *Nanoscale* **4**, 6637–6641 (2012).
18. Liu, K.-K. *et al.* Growth of large-area and highly crystalline MoS<sub>2</sub> thin layers on insulating substrates. *Nano Lett.* **12**, 1538–1544 (2012).
19. Najmaei, S. *et al.* Vapour phase growth and grain boundary structure of molybdenum disulphide atomic layers. *Nat. Mater.* **12**, 754–759 (2013).
20. Bertrand, P. A. Surface-phonon dispersion of MoS<sub>2</sub>. *Phys. Rev. B* **44**, 5745–5749 (1991).
21. Li, S. *et al.* Quantitative raman spectrum and reliable thickness identification for atomic layers on insulating substrates. *ACS Nano* **6**, 7381–7388 (2012).
22. Liu, Y. *et al.* Layer-by-layer thinning of MoS<sub>2</sub> by plasma. *ACS Nano* **7**, 4202–4209 (2013).
23. Yue, Q., Shao, Z., Chang, S. & Li, J. Adsorption of gas molecules on monolayer MoS<sub>2</sub> and effect of applied electric field. *Nanoscale Res. Lett.* **8**, 425 (2013).
24. Yavari, F. *et al.* High sensitivity gas detection using a macroscopic three-dimensional graphene foam network. *Sci. Rep.* **1**, 166 (2011).
25. Choi, H. *et al.* Flexible and transparent gas molecule sensor integrated with sensing and heating graphene layers. *Small* **10**, 3812 (2014).
26. Heyd, J., Scuseria, G. E. & Ernzerhof, M. Hybrid functionals based on a screened Coulomb potential. *J. Chem. Phys.* **118**, 8207–8215 (2003).
27. Krukau, A. V., Vydrov, O. a., Izmaylov, A. F. & Scuseria, G. E. Influence of the exchange screening parameter on the performance of screened hybrid functionals. *J. Chem. Phys.* **125**, 224106 (2006).
28. Yue, Q., Shao, Z., Chang, S. & Li, J. Adsorption of gas molecules on monolayer MoS<sub>2</sub> and effect of applied electric field. *Nanoscale Res. Lett.* **8**, 425 (2013).
29. Dolui, K., Rungger, I. & Sanvito, S. Origin of the n-type and p-type conductivity of MoS<sub>2</sub> monolayers on a SiO<sub>2</sub> substrate. *Phys. Rev. B* **87**, 165402 (2013).
30. Splendiani, A. *et al.* Emerging photoluminescence in monolayer MoS<sub>2</sub>. *Nano Lett.* **10**, 1271–1275 (2010).
31. Coehoorn, R., Haas, C. & de Groot, R. A. Electronic structure of MoSe<sub>2</sub>, MoS<sub>2</sub>, and WSe<sub>2</sub>. II. The nature of the optical band gaps. *Phys. Rev. B* **35**, 6203–6206 (1987).
32. Mak, K. F. *et al.* Tightly bound trions in monolayer MoS<sub>2</sub>. *Nat. Mater.* **12**, 207–211 (2013).
33. Mouri, S., Miyauchi, Y. & Matsuda, K. Tunable photoluminescence of monolayer MoS<sub>2</sub> via chemical doping. *Nano Lett.* **13**, 5944–5948 (2013).
34. Ross, J. S. *et al.* Electrical control of neutral and charged excitons in a monolayer semiconductor. *Nat. Commun.* **4**, 1474 (2013).
35. Mao, N., Chen, Y., Liu, D., Zhang, J. & Xie, L. Solvatochromic effect on the photoluminescence of MoS<sub>2</sub> monolayers. *Small* **9**, 1312–1315 (2013).

## Acknowledgments

This study was supported financially by the Fundamental Research Program (PNK3770 and PNK4060) of the Korean Institute of Materials Science (KIMS) and by the “Gyeongsangnam, Changwon Science Research Park Project” of the Grant of the Korean Ministry of Science, ICT and Future Planning. M. G. H. and B. C. are grateful for support from the Basic Science Research Program of the National Research Foundation of Korea (NRF) funded by the Ministry of Science, ICT & Future Planning (NRF-2014R1A1A1006214 and NRF-2014R1A1A1036139). MC was supported by Global Frontier Program through the Global Frontier Hybrid Interface Materials (GFHIM) of the National Research Foundation of Korea (NRF) funded by the Ministry of Science, ICT & Future Planning (2013M3A6B1078872).

## Author contributions

B.C., M.G.H. and D.-H.K. designed and supervised the experiments. B.C., M.G.H. and A.R.K. synthesised the MoS<sub>2</sub>. B.C., M.G.H., J.Y., A.R.K. and Y.-J.L. characterised the MoS<sub>2</sub>. B.C. and A.R.K. fabricated the MoS<sub>2</sub>-based devices. B.C., M.G.H., S.L., T.J.Y. and C.G.K. measured the MoS<sub>2</sub> sensing devices. M.G.H. and M.C. performed the first-principles DFT



calculations for the MoS<sub>2</sub> with gas molecules. B.C., M.G.H., M.C., S.-G.P., J.-D.K., C.S.K., M.S., Y.J., K.-S.N., B.H.L., H.C.K., P.M.A. and D.-H.K. analysed the data. B.C., M.G.H. and D.-H.K. co-wrote the paper. All authors discussed the results and commented on the manuscript.

### Additional information

Supplementary information accompanies this paper at <http://www.nature.com/scientificreports>

**Competing financial interests:** The authors declare no competing financial interests.

**How to cite this article:** Cho, B. *et al.* Charge-transfer-based Gas Sensing Using Atomic-layer MoS<sub>2</sub>. *Sci. Rep.* 5, 8052; DOI:10.1038/srep08052 (2015).



This work is licensed under a Creative Commons Attribution-NonCommercial-NoDerivs 4.0 International License. The images or other third party material in this article are included in the article's Creative Commons license, unless indicated otherwise in the credit line; if the material is not included under the Creative Commons license, users will need to obtain permission from the license holder in order to reproduce the material. To view a copy of this license, visit <http://creativecommons.org/licenses/by-nc-nd/4.0/>